PHYSICAL REVIEW A **90**, 053611 (2014)

Robust Ramsey sequences with Raman adiabatic rapid passage

Krish Kotru,[1,2,*] Justin M. Brown,[2] David L. Butts,[2] Joseph M. Kinast,[2] and Richard E. Stoner[2]
[1]*Department of Aeronautics and Astronautics, Massachusetts Institute of Technology, Cambridge, Massachusetts 02139, USA*
[2]*The C. S. Draper Laboratory, Cambridge, Massachusetts 02139, USA*
(Received 26 August 2014; published 10 November 2014)

We present a method for robust timekeeping in which alkali-metal atoms are interrogated in a Ramsey sequence based on stimulated Raman transitions with optical photons. To suppress systematic effects introduced by differential ac Stark shifts and optical intensity gradients, we employ atom optics derived from Raman adiabatic rapid passage (ARP). Raman ARP drives coherent transfer between the alkali-metal hyperfine ground states via a sweep of the Raman detuning through the two-photon resonance. Our experimental implementation of Raman ARP reduced the phase sensitivity of Ramsey sequences to Stark shifts in ^{133}Cs atoms by about two orders of magnitude, relative to fixed-frequency Raman transitions. This technique also preserved Ramsey fringe contrast for cloud displacements reaching the $1/e^2$ intensity radius of the laser beam. In a magnetically unshielded apparatus, second-order Zeeman shifts limited the fractional frequency uncertainty to $\sim 3.5 \times 10^{-12}$ after about 2500 s of averaging.

DOI: 10.1103/PhysRevA.90.053611 PACS number(s): 37.25.+k, 03.75.Be, 03.75.Dg

I. INTRODUCTION

Stable atomic frequency references are essential to a broad range of modern technologies, including the Global Positioning System, inertial navigators, distributed networks, and laboratory instruments. These references recently achieved an important developmental milestone with the advent of the chip-scale atomic clock (CSAC). CSACs probe narrow atomic resonances derived from coherent population trapping (CPT) of alkali-metal atoms in minute vapor cells. In a 10-cm^3 package, and with power consumption of just 100 mW [1], CSACs provide a fractional frequency stability of $2.5 \times 10^{-10}/\sqrt{\tau}$ [2,3]. Their long-term stability, however, is limited to $\sim 10^{-11}$ at 1000 s by buffer gas-dependent frequency shifts [4,5]. As a result, CSACs serve as secondary frequency references. On the other hand, state-of-the-art primary references currently realize fractional frequency uncertainties of 3×10^{-16} using laboratory-scale systems [6]. These clocks achieve high sensitivity at the expense of size and data rate, launching laser-cooled alkali-metal atoms over $\sim$1 m distances [7] and implementing microwave Ramsey sequences with long interrogation times [8,9]. Between CSACs and fountain clocks, there remains a vast, unpenetrated performance space for primary standards that operate in a compact volume and beyond the laboratory environment.

High sensitivity in fountain clocks can be traded for reduced size by shortening the Ramsey dwell time and interrogating atoms in the cooling and trapping region [10–14]. In dynamic environments, a short Ramsey time has the added benefit of reducing unconstrained motion of the atom cloud. If, for example, measurements are completed on a 10-ms time scale, a cold atom cloud experiencing 1–10-g accelerations is displaced from the trap site by $<$5 mm, enabling interferometry under dynamics, recapture of cold atoms, and fast data-rates with narrow laser beams [15,16]. The traditional method of using microwaves for the Ramsey interrogation requires well-engineered cavities or waveguides, which constrain minimum size and may be adversely affected by thermal environments or vibration [17]. An alternative approach that circumvents the cavity employs stimulated Raman transitions between alkali-metal hyperfine ground states [18]. Optical interrogation, however, introduces challenges distinct from those of microwave interrogation. Variations in the intensity of laser fields drive spurious phase shifts via the ac Stark effect [19]. Furthermore, the Gaussian intensity profile of the beam creates spatially dependent Rabi rates that, in some modalities, link Ramsey fringe contrast to radial motion of the cloud. Nevertheless, a timekeeping demonstration using CPT with optical fields recently achieved a fractional frequency uncertainty of 2×10^{-12} at 1000 s, which was limited by magnetic-field instabilities [16].

We employ a different method for optical Ramsey interrogation that suppresses sensitivity to light shifts and Rabi rate inhomogeneities [20]. Our approach uses atom optics based on Raman adiabatic rapid passage (ARP) [21], which is inspired by, and isomorphic to, ARP techniques used by the nuclear magnetic resonance (NMR) community [22,23]. In NMR, ARP inverts the population in a two-level system by slowly sweeping the angular frequency of a rotating magnetic field through the Rabi resonance [24]. In the frame of the time-dependent field, the nuclear spin precesses about the effective magnetic field with a latitude that slowly tilts from the north to south pole. Our approach with Raman ARP requires an analogous sweep of the frequency difference of the Raman optical fields through the two-photon resonance. Raman ARP reduces the phase sensitivity of a Ramsey sequence to the differential ac Stark shift, because the first beamsplitter does not imprint a relative phase on the quantum state in the adiabatic limit, as will be discussed below. ARP is also robust to intensity variations, since transfer efficiency is not a strong function of Rabi rate. As a result, interferometer contrast is preserved in the presence of intensity fluctuations and gradients, and the phase is insensitive to small changes in frequency sweep parameters.

Raman ARP differs in important respects from stimulated Raman adiabatic passage (STIRAP), in which adiabatic transfer in a three-level system results from the time-delayed intensity modulation of two optical fields. Experimental

*kotru@mit.edu

demonstrations of STIRAP have produced coherent transfer of alkali-metal atoms between hyperfine ground states and targeted Zeeman sublevels, as well as useful atom interferometers [25,26]. Frequency-swept ARP has two advantages over STIRAP: In a Ramsey sequence, spontaneous emission during the second STIRAP pulse reduces the maximum interferometer contrast by approximately a factor of 2; the presence of multiple excited levels in alkali-metal atoms reintroduces residual Stark shifts to STIRAP, with dependencies on pulse duration, optical intensity, and single-photon laser detuning [27].

In this work, we experimentally demonstrated efficient population inversion and Ramsey interferometry based on Raman ARP, described in Secs. III and IV, respectively. We also studied effects of the ac Stark shift and optical intensity of the Raman fields on the phase and contrast of Ramsey interferograms. In Sec. V A, we show that Raman ARP suppressed phase deviations due to ac Stark shifts by about two orders of magnitude, compared to fixed-frequency Raman transitions. Section V B discusses the Gaussian spatial intensity distribution of the Raman beam, which induced fractional variations in contrast that were a factor of 15 smaller (over half the $1/e^2$ intensity radius) for Raman ARP than for standard Raman transitions. Deliberate perturbations ($\pm 10\%$) to parameters defining the ARP frequency sweeps did not introduce resolvable shifts in phase, as shown in Sec. V C. Finally, Sec. VI presents a preliminary stability assessment of Raman ARP Ramsey interrogations. In a laboratory setting—but without magnetic shielding—our apparatus achieved a fractional frequency uncertainty that was limited by second-order Zeeman shifts to 3.5×10^{-12} after 2500 s of averaging.

II. RAMAN SPECTROSCOPY WITH COLD ATOMS

To investigate Ramsey sequences based on Raman ARP, we worked exclusively with the D2 line in ^{133}Cs atoms. Interferometry experiments occurred inside an octagonal, 80-cm^3, machined-quartz cell, which maintained a background vapor pressure of 10^{-9} Torr [Fig. 1(a)]. Environmental magnetic fields were canceled by three orthogonal pairs of Helmholtz coils. Each measurement cycle began with the cooling and trapping of $\sim 10^7$ atoms in 600 ms using a magneto-optical trap. Polarization gradient cooling further cooled the cloud to 9 μK. To prepare the atoms in a single hyperfine ground state, we first applied a vertical bias field of 0.87 G that lifted the Zeeman degeneracy. The atoms were then optically pumped on the $|F = 4\rangle \rightarrow |F' = 4\rangle$ transition (F' denotes a hyperfine level in the $6^2P_{3/2}$ manifold) with light polarized linearly and parallel to the bias field until 90% of the atoms were in the $|F = 4, m_F = 0\rangle$ dark state. Light resonant with the $|F = 3\rangle \rightarrow |F' = 4\rangle$ transition simultaneously pumped atoms out of $F = 3$. A microwave π pulse tuned to the clock transition transferred atoms from the dark state to $|F = 3, m_F = 0\rangle$. A subsequent laser pulse, resonant with the $|F = 4\rangle \rightarrow |F' = 5\rangle$ cycling transition, pushed atoms remaining in $F = 4$ out of the interaction region. Interferometry began with >97% of the remaining atoms initially in the $|F = 3, m_F = 0\rangle$ clock state. These atoms were interrogated in a Ramsey sequence, which comprised two atom "beamsplitters" (e.g., Raman $\pi/2$ pulses) separated by an interrogation time T that ranged from 1 to 17 ms. The final state of the interferometer consisted of atoms in superpositions of the $F = 3$ and $F = 4$ clock states. To extract the interferometer phase, we measured the fraction of atoms in $F = 4$ after laser induced fluorescence. Specifically, we applied light resonant with the $|F = 4\rangle \rightarrow |F' = 5\rangle$ transition, and associated the resulting fluorescence with states that had collapsed to $F = 4$. A second pulse of the same light then pushed these atoms out of the interaction region. The remaining atoms in $F = 3$ were optically pumped to $F = 4$ and fluoresced in a similar manner. The sum of these two fluorescence signals was proportional to the total population and the ratio of total fluorescence to fluorescence from the $F = 4$ atoms provided a normalized readout. A more detailed description of atom trapping and state preparation in our apparatus can be found in Refs. [28,29].

We drove the ^{133}Cs clock transition ($|F = 3, m_F = 0\rangle \rightarrow |F = 4, m_F = 0\rangle$) using stimulated Raman processes via intermediate excited states in the $6^2P_{3/2}$ manifold [Fig. 1(b)]. The Raman optical frequencies, ω_1 and ω_2, were generated by phase modulating the output of an external cavity diode laser with an electro-optic modulator (EOM). The optical spectrum contained frequency sidebands spaced about the carrier by integer multiples of the Zeeman-shifted hyperfine splitting frequency $\omega_{\mathrm{HFS}}/2\pi = 9\,192\,631\,770 + 324$ Hz. To reduce spontaneous emission, we blue-detuned the Raman laser by 2.02 GHz with respect to the $|F = 3\rangle \rightarrow |F' = 4\rangle$ transition. At this detuning, the differential ac Stark shift (i.e., the difference of the ac Stark shifts of the clock states) was canceled when the optical power was $\sim 10\%$ larger in the carrier frequency than in each first-order sideband. To obtain agile control over the microwave signal that drove the EOM, we used a single-sideband mixer (Polyphase SSB90110A) to combine the 30-MHz output of a 625-MS/s arbitrary waveform generator (Agilent N8241A) with a constant 9.163-GHz signal (Agilent E8257D). The phase, frequency, and power of the resulting rf signal were controlled through the waveform generator, enabling rapid frequency sweeps for Raman ARP. An acousto-optic modulator placed before the EOM switched

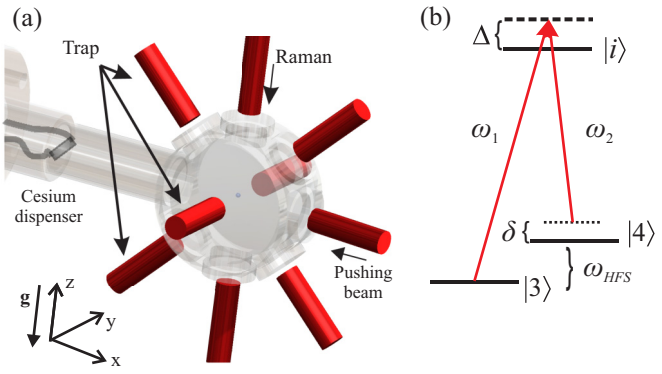

FIG. 1. (Color online) (a) Octagonal glass vacuum chamber and laser beam configuration for atom trapping, state preparation, and interferometry. During experiments, atoms fall through the center of the Raman beam because of its vertical orientation. (b) ^{133}Cs ground-state energy levels $|3\rangle$ and $|4\rangle$ coupled by a stimulated Raman transition with single-photon detuning Δ, Raman detuning δ, and optical frequencies ω_1 and ω_2.

the Raman light in 50 ns, and a tapered amplifier downstream of the EOM increased the total Raman optical power presented to the atoms to 40 mW. The optical spectrum of the tapered amplifier contained a 30-nm-wide pedestal carrying a small amount of resonant light. To reduce spontaneous emission during the interferometer, we filtered the resonant light from the pedestal by passing the output of the tapered amplifier through a Cs reference vapor cell. The Raman beam was vertically oriented, circularly polarized, and delivered to the cell using a fiber-coupled collimator with 7.1-mm $1/e^2$ intensity diameter. The co-propagating pair of carrier and -1 sideband frequencies drove the dominant Raman transition, which was Doppler shifted by 30.7 Hz/(m/s), or 0.3 Hz/ms in a 1-g environment.

Interferometry experiments generally involved extracting interferograms while deliberately varying parameters like the differential ac Stark shift or the two-photon Rabi rate. To generate an interferogram, we typically measured the transition probability while shifting the laser phase difference between the Raman optical fields. This phase difference was scanned over 17 values in steps of $\pi/4$ rad, and the transition probability at each phase was measured five times consecutively to enable averaging. With a per-shot data rate of 1.6 Hz, a full interferogram was acquired every 53 s. To isolate slow systematic variations due to oscillator drift and environmental magnetic fields, interferograms for ARP, Raman, and microwave pulses were acquired consecutively, within 2.7 min, at a particular parameter setting. Parameters were varied nonmonotonically to further reduce contributions from slow systematic trends. Finally, we cycled through the parameter values of interest three times for additional averaging.

III. RAMAN ADIABATIC RAPID PASSAGE

Frequency-swept ARP is a standard tool for robust population inversion in NMR. Its effect on a two-state system can be visualized on the Bloch sphere shown in Fig. 2. The pseudospin polarization $\hat{\mathbf{p}}$ represents a superposition of spin-up and spin-down states, which correspond to $|F=4,m_F=0\rangle$ and $|F=3,m_F=0\rangle$, respectively. The generalized Rabi rate $\vec{\mathbf{\Omega}}_{\rm gen}$ represents the Raman pulse, or "drive field," and is analogous to the effective magnetic field in the traditional NMR problem. When the drive field is applied, $\hat{\mathbf{p}}$ precesses about $\vec{\mathbf{\Omega}}_{\rm gen}$ at the generalized Rabi frequency $\Omega_{\rm gen}=\sqrt{\Omega_{\rm eff}^2+\delta^2}$, where $\Omega_{\rm eff}$ is the magnitude of the two-photon Rabi rate, and $\delta=\omega_1-\omega_2-\omega_{\rm HFS}$ is the Raman detuning. The polar angle of the drive field is defined as $\theta=-\arctan(\Omega_{\rm eff}/\delta)$. The azimuthal angle φ represents the phase difference between the two Raman frequency components. If the drive field is rotated at a rate $\dot{\theta}\ll\Omega_{\rm gen}$, $\hat{\mathbf{p}}$ encircles $\vec{\mathbf{\Omega}}_{\rm gen}$ before θ can change appreciably. As a result, rapid precession causes $\hat{\mathbf{p}}$ to adiabatically follow $\vec{\mathbf{\Omega}}_{\rm gen}$. The projection of $\hat{\mathbf{p}}$ onto the drive field, which we define as $\vec{\mathbf{p}}_{\parallel}$, can thus be dragged anywhere on the sphere. Experimentally, we control θ by sweeping δ through resonance, over a frequency range that is large with respect to $\Omega_{\rm eff}$. We note that a two-state model is appropriate for this work because the single-photon detuning Δ is much larger than $\Omega_{\rm eff}$. This parameter regime allows for adiabatic elimination of all intermediary excited states in the $6^2P_{3/2}$ manifold [30].

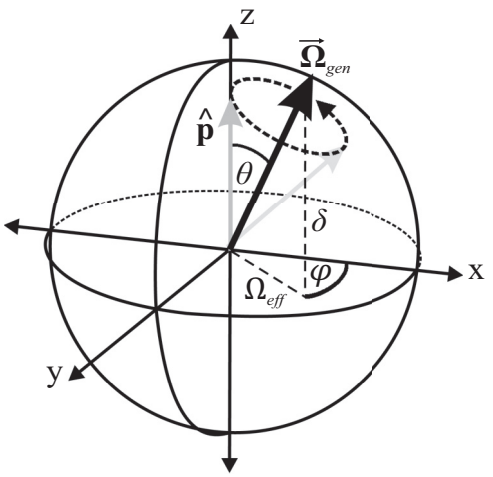

FIG. 2. Bloch sphere depiction of Raman adiabatic rapid passage. The pseudospin polarization $\hat{\mathbf{p}}$ adiabatically follows $\vec{\mathbf{\Omega}}_{\rm gen}$ when $\dot{\theta}\ll\Omega_{\rm gen}$, where $\Omega_{\rm gen}$ is the rate of precession of $\hat{\mathbf{p}}$ about $\vec{\mathbf{\Omega}}_{\rm gen}$.

ARP is generally advantageous when inversion is required in the presence of an inhomogeneous drive field [22,31]. Since the Rabi rate in this case is position dependent, precise control of spin precession cannot be achieved simultaneously over the entire ensemble. As a result, fixed-frequency π and $\pi/2$ pulses tend to over- or undershoot the desired pulse area for a given atom. With an ARP sweep, however, transfer efficiency in the adiabatic limit ultimately depends on the projection of $\hat{\mathbf{p}}$ onto $\vec{\mathbf{\Omega}}_{\rm gen}$, namely $\vec{\mathbf{p}}_{\parallel}$, which is independent of precession. In the standard approach to ARP, $\delta(t)$ is linearly chirped through resonance. For this work, we instead chose a nonlinear sweep that rapidly changed the polar angle θ at the beginning and end of the adiabatic passage, when the adiabatic condition was well satisfied. A short sweep helps minimize dephasing due to spontaneous emission. Our frequency sweep is described by the equation

$$\delta(t)=\Omega_{\rm arp}\tan\left[\alpha\left(\frac{2t}{T_\pi}-1\right)\right],\quad t\in\{0,T_\pi\},\qquad(1)$$

where T_π sets the total sweep duration, $\Omega_{\rm arp}$ controls the sweep rate without perturbing its duration or range, and $\alpha=\arctan(\delta_{\rm max}/\Omega_{\rm arp})$, where $\delta_{\rm max}$ is the maximum detuning. To quantify the adiabaticity of a particular sweep, we define the unitless parameter $Q(t)=\Omega_{\rm gen}/|\dot{\theta}|$. Near resonance, and when $\delta_{\rm max}\gg\Omega_{\rm eff}=\Omega_{\rm arp}$, Q is equivalent to T_π in units of Raman π pulses. In other words, $Q=n$ when $T_\pi=nt_\pi$, where t_π is the duration of a Raman π pulse. Previous work has shown that $Q\geqslant 5$ provides sufficient adiabaticity for robust population transfer [32]. Since the present work is focused on interferometry, in which the sweeps begin or end near resonance (when Q is minimized), we consider more adiabatic sweeps with $Q=10$ and 26. The frequency sweep described by Eq. (1) is coupled with an intensity modulation $I(t)$ of the form

$$I(t)=I_0\tanh\left[\beta\left(1-\left|\frac{2t}{T_\pi}-1\right|\right)\right],\qquad(2)$$

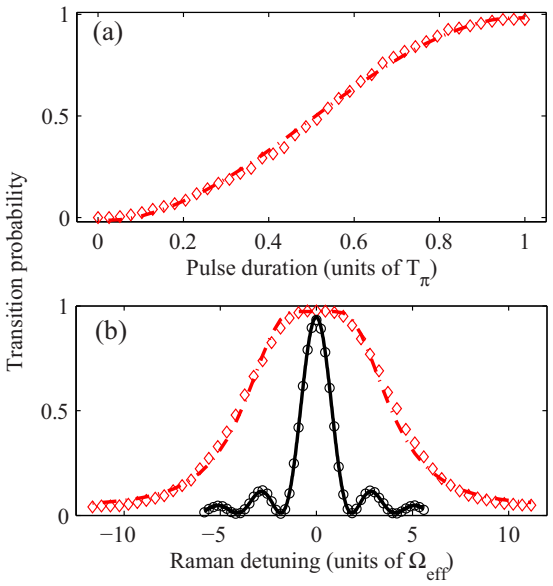

FIG. 3. (Color online) (a) Time evolution of the transition probability during the Raman ARP sweep described by Eqs. (1) and (2). The sweep parameters were $T_\pi = 10.3t_\pi$, $\delta_{max}/2\pi = 15$ MHz, and $\Omega_{arp}/2\pi = \Omega_{eff}/2\pi = 86$ kHz. (b) Scanning the Raman ARP center frequency (red diamonds) with the same sweep parameters used above produces a Raman resonance with linewidth five times broader than that of a Raman π pulse (black circles). All lines represent predictions based on a model of a two-level atom.

where I_0 is the maximum intensity, and the unitless parameter β is typically 7.5. Since $I(0) = I(T_\pi) = 0$, the drive field at the beginning and end of the sweep is essentially parallel with the z axis of the Bloch sphere. This alignment helps maximize transfer efficiency when atoms are prepared in one of the clock states. Variants of this sweep have been proposed and implemented in Refs. [32–34].

Figure 3(a) shows the ensemble-averaged time evolution of the transition probability during this tangent sweep. For $\Omega_{eff} = \Omega_{arp}$, the measured transition probabilities follow the sinusoid predicted by our model (described below). Measurements of the transition probability as a function of the center frequency of the sweep, shown in Fig. 3(b), reveal a full width at half maximum of $8\Omega_{eff}$, which is about five times broader than the corresponding bandwidth of a Raman π pulse. Near resonance, the coherent transfer efficiency is limited to 93% by spontaneous emission. Agreement between the measurements and model helped validate our hardware implementation of Raman ARP.

The predictions plotted in Fig. 3 were based on a model of a two-level atom. The dynamics of this system, viewed in the reference frame of Fig. 2, are given by the equation

$$\frac{d\hat{\mathbf{p}}}{dt} = \vec{\mathbf{\Omega}}_{gen} \times \hat{\mathbf{p}}. \tag{3}$$

With a set of initial conditions for the drive field and the pseudospin polarization, the model numerically integrates Eq. (3). Numerical integration is necessary because Raman ARP frequency sweeps introduce time dependencies to $\vec{\mathbf{\Omega}}_{gen}$ that generally preclude analytic solutions. The framework can be extended to model interferometer sequences by incorporating a period of free precession about the z axis of the Bloch sphere during the time between two pulses. Following a pulse sequence, the model reports the atom transition probability in response to a varied parameter (e.g., Raman detuning or phase). The model is also capable of accounting for ensemble effects by repeating the calculation for many atoms with randomly assigned positions and velocities, making Ω_{eff} a Gaussian function of position, and averaging over the resulting transition probabilities. In this work, predictions from our model do not include ensemble averaging effects.

IV. INTERFEROMETRY WITH RAMAN ARP

Ramsey sequences are commonly viewed as atom interferometers comprising two $\pi/2$ pulses, or beamsplitters, separated by an interrogation time T. An atom beamsplitter divides the atomic wave packet in two, with the resulting partial wave packets assuming different hyperfine and momentum states. In practice, the co-propagating Raman optical fields used in this work impart a negligible momentum kick. A Ramsey sequence derived from these beamsplitters is then primarily an atom interferometer for the internal hyperfine states of the atom. Raman ARP serves as an effective beamsplitter for a Ramsey atom interferometer when the sweep is stopped midway, at the Raman resonance [21]. In Fig. 4(a), the first Ramsey pulse begins with $\vec{\mathbf{\Omega}}_{gen}$ and $\hat{\mathbf{p}}$ initially parallel. The drive field then slowly drags the pseudospin into the x-y plane [see Fig. 4(b)], creating a coherent superposition

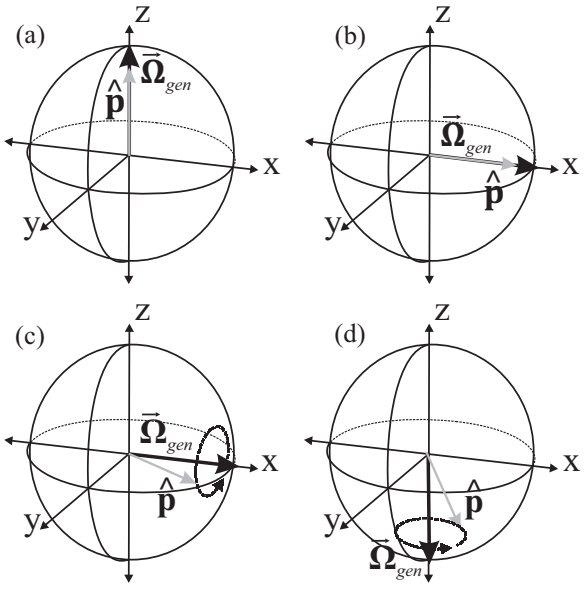

FIG. 4. Raman ARP Ramsey sequence on the Bloch sphere. (a) Following state preparation, $\vec{\mathbf{\Omega}}_{gen}$ is parallel to $\hat{\mathbf{p}}$. (b) The first sweep transfers the pseudospin polarization into the x-y plane when its center frequency matches the Raman resonance condition. (c) After a Ramsey interrogation time T, the second beamsplitter generally begins with nonparallel $\vec{\mathbf{\Omega}}_{gen}$ and $\hat{\mathbf{p}}$, which leads to precession of $\hat{\mathbf{p}}$ about $\vec{\mathbf{\Omega}}_{gen}$. (d) The second beamsplitter drags $\vec{\mathbf{p}}_\parallel$ to the z axis, mapping the relative phase between the drive field and pseudospin polarization to population difference.

of the clock states. After an interrogation time T, a second beamsplitter starts nearly on resonance to complete the Ramsey sequence. At the beginning of this pulse, $\vec{\mathbf{\Omega}}_{\rm gen}$ and $\hat{\mathbf{p}}$ are generally nonparallel, because of discrepancies between the oscillator and atomic resonance frequencies—which the atomic reference is intended to correct. The misalignment leads to the precession shown in Fig. 4(c). The drive field then drags $\vec{\mathbf{p}}_{\parallel}$ to the z axis [Fig. 4(d)], thereby converting the interferometer phase into population difference.

Rapid completion of this pulse sequence is beneficial for a device operating in dynamic environments. A short measurement sequence ensures that an atom cloud experiencing large transverse acceleration remains within the Raman laser beam during the Ramsey interrogation. It also enables averaging of noise processes to lower levels in shorter times, thereby affording excellent short-term sensitivity. For example, an interrogation time of $T = 10$ ms, coupled with a sampling rate of $f_s = 80$ Hz and a phase signal-to-noise ratio of $\mathrm{SNR}_\phi = 200$, results in a fractional frequency stability of

$$\frac{1/\mathrm{SNR}_\phi}{\omega_{\rm HFS} T \sqrt{f_s}} \approx 1 \times 10^{-12} \tag{4}$$

for an averaging time of 1 s. Moreover, the cloud remains within the $1/e^2$ intensity radius of the Raman beam for transverse accelerations up to 5 g. Figure 5 shows examples of Ramsey fringes based on Raman $\pi/2$ pulses and Raman ARP beamsplitters with $T_\pi = 10t_\pi$ and $26t_\pi$. The interrogation time was $T = 10$ ms, the magnitude of the two-photon Rabi rate was $\Omega_{\rm eff}/2\pi = 73$ kHz, and the ARP sweep parameters were $\delta_{\rm max}/2\pi = 15$ MHz and $\Omega_{\rm arp}/2\pi = 73$ kHz. To reduce discrepancies arising from oscillator drifts and environmental magnetic fields, the three pulse types were applied sequentially at a given detuning, and measurements were collected at 1.6 Hz over 10 min. The measurements were fit to a cosine function given by

$$P = \frac{1}{2} + \frac{A}{2}\cos[(\delta - \delta_0)T] + B, \tag{5}$$

where P was the measured transition probability, and free parameters such as contrast A, background offset B, and Raman detuning offset δ_0, were determined through minimization of the sum of squares of the residuals. For both the Raman $\pi/2$ and $T_\pi = 26t_\pi$ cases, the fit uncertainty in $\delta_0/2\pi$ was ± 0.24 Hz, indicating similar short-term stability.

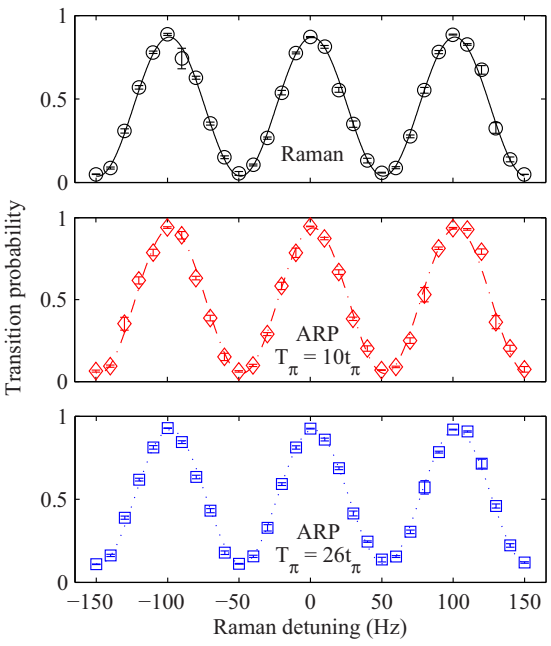

FIG. 5. (Color online) Ramsey fringes with an interrogation time of $T = 10$ ms. Lines are best-fit cosine functions and points are measured values. At a given detuning, the three pulse types were applied sequentially, and measurements were collected at 1.6 Hz over 10 min. The condition $\delta = 0$ includes a Zeeman shift of 324 Hz. Uncertainty in the frequency offset $\delta_0/2\pi$ was ± 0.24 Hz for the Raman and $T_\pi = 26t_\pi$ cases, indicating comparable short-term stability.

Raman ARP Ramsey sequences are insensitive to dynamic phase associated with pseudospin precession in the adiabatic limit. The source of dynamic phase becomes clear in the dressed-atom basis [21]. Eigenstates in this basis are parallel and antiparallel to $\vec{\mathbf{\Omega}}_{\rm gen}$, with eigenenergies of $\pm\hbar\Omega_{\rm gen}/2$. When $\vec{\mathbf{\Omega}}_{\rm gen}$ is varied adiabatically, a dressed eigenstate acquires a phase $\gamma = \pm\int_0^t \Omega_{\rm gen}(t')dt'/2$, in a manner analogous to the evolution of eigenstates in a time-independent system. During the first ARP beamsplitter, $\hat{\mathbf{p}}$ is the dressed eigenstate parallel to $\vec{\mathbf{\Omega}}_{\rm gen}$, so adiabatic evolution introduces an undetectable overall phase γ_1. For subsequent pulses, however, $\vec{\mathbf{\Omega}}_{\rm gen}$ and $\hat{\mathbf{p}}$ are typically nonparallel [Fig. 4(c)]. The state is therefore a superposition of dressed eigenstates, which acquire differential phases $\pm\gamma_2$ during the sweep. The two-pulse Ramsey sequence is insensitive to this relative dynamic phase, because γ_2 remains a phase prior to state readout. Interferometers involving more than two beamsplitters map dynamic phases to population difference if subsequent ARP sweeps do not cancel them (e.g., by reversing the direction of $\vec{\mathbf{\Omega}}_{\rm gen}$). In this case, inhomogeneities in $\Omega_{\rm eff}$ and δ may dephase the ensemble and wash out interference fringes.

V. SYSTEMATIC EFFECTS

A cold atom frequency standard based on Ramsey sequences is likely to experience parameter fluctuations during operation outside the laboratory. In dynamic environments, variations in optical power, rf power, and atom cloud position could systematically affect Ramsey interferograms. In this section, we demonstrate how Raman ARP beamsplitters in a Ramsey sequence suppress some of these systematic effects.

A. Light shifts during a pulse

A Ramsey sequence based on Raman ARP affords an important advantage over Raman $\pi/2$ pulses: light shifts during a pulse leave the interferometer phase unperturbed. The presence of a light shift during Raman ARP moves the center frequency of the sweep off resonance. The beamsplitter shown in Fig. 4(b) ends outside the x-y plane, as does the parallel pseudospin $\hat{\mathbf{p}}$. This error in polar angle does not affect the phase of the Ramsey interferometer, which instead depends on the azimuthal separation between $\hat{\mathbf{p}}$ and $\vec{\mathbf{\Omega}}_{\rm gen}$. Errors in polar

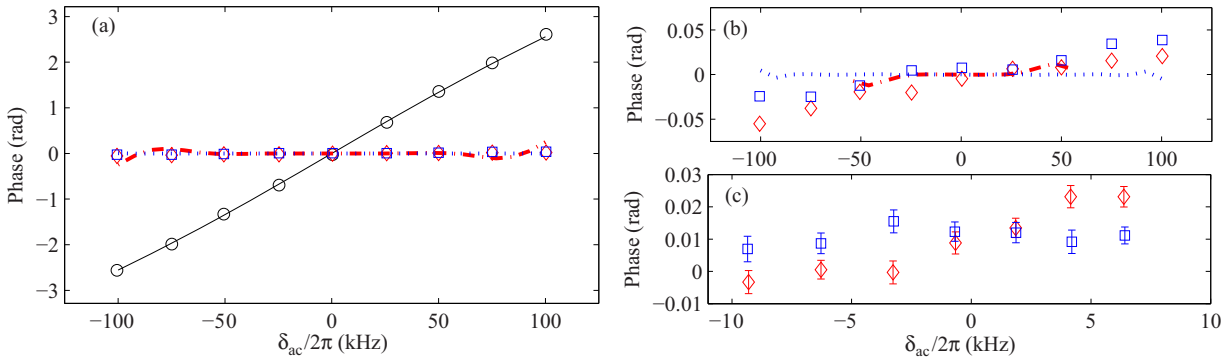

FIG. 6. (Color online) (a) Large-scale sensitivity of Ramsey phase to differential ac Stark shifts. The Raman pulse case (black circles and solid line) was about 75 times more sensitive to δ_{ac} than Raman ARP interrogations with $T_\pi = 10t_\pi$ (red diamonds) and $T_\pi = 26t_\pi$ (blue squares). All lines are based on a model. (b) A detailed view of Raman ARP measurements reveals residual phase variations not predicted by our model. Predictions for Raman ARP with $T_\pi = 10t_\pi$ (red dash-dot line) are restricted to detunings where the model produced controlled phase shifts. (c) Sensitivity of Raman ARP interrogations to the smaller differential ac Stark shifts expected in a practical device. In this regime, the Raman pulse case was roughly 100 times more sensitive to δ_{ac} than Raman ARP interrogations with $T_\pi = 26t_\pi$.

angle, however, do affect interferometer contrast. When the second beamsplitter is initially π rad out of phase with $\hat{\mathbf{p}}$, the light shift reduces the transfer efficiency, causing the troughs of the interferogram to rise up. For the small light shifts relevant to a practical device, we show that the resulting variations in contrast and background offset have a minor impact on sensitivity.

We tested the sensitivity of three types of Ramsey sequences to the differential ac Stark shift δ_{ac}. In particular, we compared Raman $\pi/2$ pulse sequences to Raman ARP sequences with T_π durations of $10t_\pi$ and $26t_\pi$, recording contrast A, background offset B, and systematic phase offset Φ for each interferogram. The transition probability P is related to these quantities by Eq. (5), where the detuning dependence in the argument of the cosine function is replaced by $\Phi + \Delta\varphi$, and $\Delta\varphi$ is the programed phase difference between the two Ramsey pulses. We extracted entire interferograms to determine A, B, and Φ simultaneously, which suppressed undesirable cross-coupling effects in the measurement of P. This technique differs from a simpler one in which each measurement of phase is related to a single measurement of transition probability made with $\Delta\varphi = \pi/2$ and $\Phi \approx 0$. In that approach, phase measurements are susceptible to variations in A and B since the transition probability varies with these parameters [see Eq. (5)].

For each δ_{ac} setting, the three types of interferometers were measured sequentially, three times over 8 min. To extract an interferogram, $\Delta\varphi$ was scanned over two fringes in steps of $\pi/4$ rad (to enable averaging, each phase condition was repeated five times, consecutively). We controlled δ_{ac} with the modulation depth of the EOM in the Raman beam path, which adjusted the ratio of the optical powers in each Raman frequency. At each setting of the modulation depth, the overall optical power was adjusted with the tapered amplifier to maintain $\Omega_{eff}/2\pi = 73$ kHz to within $\pm 2\%$. The light shift was assumed to be the Raman detuning at which population transfer with a Raman π pulse was maximized. Following these calibration steps, the oscillator frequency was set to the Zeeman-shifted clock resonance before interferometry commenced. In doing so, the oscillator was detuned by the light shift during application of the pulse, but resonant with the atoms during the Ramsey dwell period. The short $T = 1$ ms interrogation time suppressed the sensitivity to oscillator instabilities and helped isolate phase shifts associated with pulse dynamics.

Figure 6(a) shows the systematic phase offset Φ of each interferometer as a function of δ_{ac}. The Raman-pulse measurements show good agreement with the predictions from our model. Linear fits to the predictions and measurements give a light shift sensitivity of 26 mrad/kHz. The ARP interferometers strongly suppress this sensitivity. A closer view of the Raman ARP data, shown in Fig. 6(b), reveals an overall linear trend of 0.34 mrad/kHz with localized curvature, neither of which our model predicts. The predictions for $T_\pi = 10t_\pi$ (red dash-dot curve) are restricted to detunings where the sweep is adiabatic enough for the model to produce controlled phase shifts. That the corresponding measured phases at $\delta_{ac}/2\pi = \pm 100$ kHz are not completely randomized may result from ensemble averaging effects.

In practice, the differential Stark shift, with $\Delta \approx 2$ GHz, will likely be restricted to $\pm 0.02\Omega_{eff} \approx \pm 2\pi \times 1$ kHz, due to $\sim 1\%$ power fluctuations in the rf signal modulating the EOM; below this bound, the measurement and stabilization of rf power is challenging. We therefore repeated this experiment over a narrower detuning range near $\delta_{ac} = 0$, using the data acquisition procedure described in Sec. II. In this case, Ω_{eff} was not calibrated from one condition to the next, because the measured variation was just $\pm 2\%$ of the nominal setting. The light shift was calibrated to the modulation depth of the EOM, which was then tracked via real-time rf power measurements. Linear fits to the Raman ARP phase offsets, which are shown in Fig. 6(c), and the Raman phase offsets (not shown) were compared to determine the *relative* sensitivity to δ_{ac}. The ratios of the two ARP slopes to the Raman slope were 0.063 ± 0.008 for the $T_\pi = 10t_\pi$ case and 0.005 ± 0.008 for the $T_\pi = 26t_\pi$ case. Since drifts in δ_{ac} on the order of $\pm 0.02\Omega_{eff}$ are expected in a practical device, the measured sensitivity of the Raman $\pi/2$ sequence to δ_{ac} implies that the phase will drift by 26 mrad. In the case where δ_{ac} is a white noise process, the fractional frequency stability for the example presented in Eq. (4) becomes 5×10^{-12} after 1 s

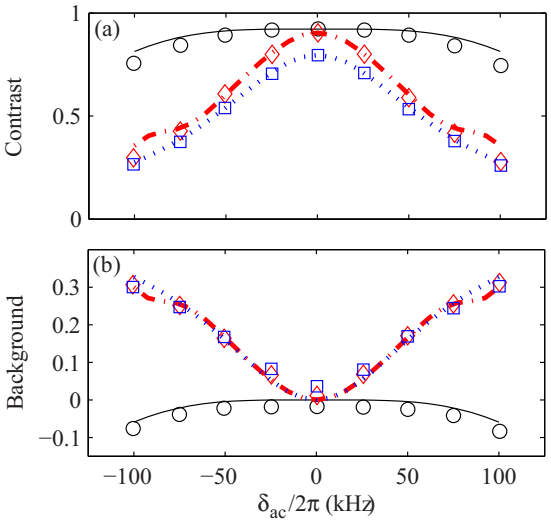

FIG. 7. (Color online) Sensitivity of (a) contrast and (b) background offset to differential ac Stark shifts for Ramsey sequences based on Raman (black circles), Raman ARP with $T_\pi = 10t_\pi$ (red diamonds), and Raman ARP with $T_\pi = 26t_\pi$ (blue squares) beamsplitter pulses. Lines represent predictions from a model. For small δ_{ac}, the ARP offsets should vary by 0.07%, leading to a phase error (<2 mrad) below the expected signal-to-noise ratio of a practical system. This error could be further suppressed by alternating phase measurements at $\Delta\varphi = \pm\pi/2$.

of averaging, because the phase signal-to-noise ratio drops to $\mathrm{SNR}_\phi = 40$. By comparison, the Raman ARP interferometer with $T_\pi = 26t_\pi$ brings the noise process due to ac Stark shifts below the atom shot noise limit for 10^7 atoms.

The extraction of full interferograms also enabled the study of contrast and background offset variations in response to the light shift. When phase shifts are estimated from single measurements of transition probability, made near $\Delta\varphi = \pi/2$, variations in background offset can lead to large apparent phase shifts. Small changes in contrast, however, are inherently tolerable near $\Delta\varphi = \pi/2$, since they merely scale existing errors in transition probability [see Eq. (5)]. Figure 7(a) shows the contrast response to δ_{ac} for the three pulses considered above. In each case, the maximum measured contrast serves to normalize the associated predictions. This normalization qualitatively accounts for spontaneous emission losses during Raman ARP sweeps and yields good agreement with measurements when the sweep is adiabatic. For Raman pulses, normalization approximately accounts for dephasing due to inhomogeneities in Ω_{eff} and δ_{ac} (spontaneous emission makes a minor contribution). Since these inhomogeneities scale with Ω_{eff} and δ_{ac} and are coupled, it is reasonable that the model overestimates the contrast away from resonance. For small differential Stark shifts of $\pm 0.02\Omega_{\mathrm{eff}}$ (within the bounds of reasonable rf power control), the contrast is expected to vary by about 0.13% and should scale phase deviations from $\Delta\varphi = \pm\pi/2$ by this fraction.

Variations in background offsets follow the unmodified predictions of our model, as shown in Fig. 7(b). The rise in Raman ARP offsets in response to detuning indicates that the troughs of the interferograms are pulled up due to impaired transfer efficiency during the second pulse. For Stark shifts of $\pm 0.02\Omega_{\mathrm{eff}}$, the offset is expected to vary by about 0.07%, leading to <2 mrad error in phase and a fractional frequency stability at 1 s of 3×10^{-13}—a minor contribution to SNR_ϕ [see Eq. (4)]. Sensitivity to background offsets can be further suppressed by sequentially measuring transition probability near $\Delta\varphi = \pm\pi/2$ and estimating the phase error from the difference of consecutive measurements. Slow variations in this parameter are then immaterial since they produce the same differential phase.

B. Laser beam intensity profile

Raman ARP also achieves a high degree of robustness against optical intensity variations. Since $\tilde{\mathbf{p}}_\parallel$ is unaffected by Ω_{eff} in the adiabatic limit, Ramsey sequences based on Raman ARP maintain high contrast despite fluctuations in optical power or poor beam quality. An important cause of power variation, particularly on dynamic and mobile platforms, is motion of the atom cloud along the beam radius. During a $T = 10$ ms interrogation, for instance, a cloud accelerating transverse to the beam axis at 3.5 g traverses the 1σ radius of a Gaussian beam with a 7-mm $1/e^2$ intensity diameter. Over this distance, the beam profile introduces substantial position-dependent changes to the gradient and average of the optical intensity experienced by the cloud. A practical timing reference might measure such accelerations using an inertial sensor. With a $T = 10$ ms interrogation time, a low-performance accelerometer with 10-mg resolution can determine the radial position of the cloud to within 5 μm. Such accurate position information, along with knowledge of the beam profile, enables compensation for changes in the average intensity via modification of optical power or pulse duration.

Optical intensity gradients, however, are more challenging to correct in real time. An alternative approach is to provide uniform intensity with a "flat-top" beam. Unfortunately, uniform intensity only occurs in a small region along the propagation axis of this beam, and the resulting optical wavefronts are distorted. Being limited to a Gaussian beam, we tested the effect of the intensity gradient on interferometer contrast by displacing the Raman beam relative to the atom cloud and using pulse duration to compensate for changes in the average intensity. Specifically, we corrected pulse durations at each position so that $t_\pi = \pi/\Omega_{\mathrm{eff}}$. During real transverse accelerations, the first Ramsey pulse occurs with the cloud near beam center, while the second occurs with the cloud closer to the beam edge, where the gradients are larger. In our experiments, conditions were more adverse: the Raman beam position was kept constant for a given experimental condition, meaning both pulses imposed deleterious intensity gradients.

To control the radial position of the cloud within the beam, the Raman beam collimator was mounted to a linear translation stage. Prior to the experiment, the beam was centered on the cloud by maximizing Ω_{eff} with a fixed optical intensity, and then minimizing decoherence during Rabi flopping experiments. Ω_{eff} and δ_{ac} were extracted at each position from measurements of the Raman π pulse resonance as a function of detuning [e.g., Fig. 3(b)], and the differential ac

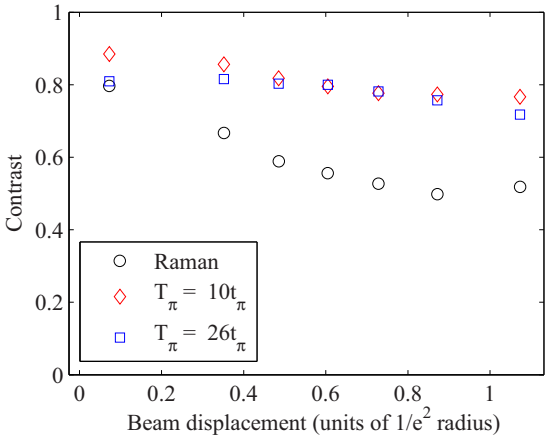

FIG. 8. (Color online) Contrast variation due to laser beam intensity gradients for Ramsey sequences based on Raman (black circles), Raman ARP with $T_\pi = 10t_\pi$ (red diamonds), and Raman ARP with $T_\pi = 26t_\pi$ (blue squares) beamsplitter pulses. To change the intensity gradient, a Raman beam with Gaussian intensity profile was displaced relative to the cloud. To compensate for changes in the average intensity, we adjusted pulse durations so that $t_\pi = \pi/\Omega_{\text{eff}}$ at each position. Over the $e^{-1/2}$ intensity radius, the fractional variation in contrast was 15 times larger for Raman $\pi/2$ pulses than for Raman ARP with $T_\pi = 26t_\pi$.

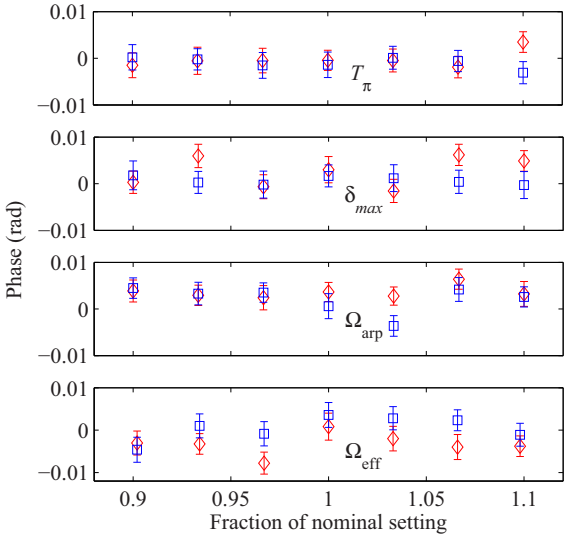

FIG. 9. (Color online) Phase sensitivity of Raman ARP Ramsey sequence to 10% variations in parameters defining the ARP frequency sweep. Nominal settings: $T_\pi = 10t_\pi$ (red diamonds) or $T_\pi = 26t_\pi$ (blue squares), $\delta_{\text{max}}/2\pi = 15$ MHz, $\Omega_{\text{arp}}/2\pi = 73$ kHz, and $\Omega_{\text{eff}}/2\pi = 73$ kHz. The residual instability in these measurements was driven largely by magnetic-field fluctuation.

Stark shift was reduced to $|\delta_{\text{ac}}| \leqslant 0.02\Omega_{\text{eff}}$. The ARP sweeps were adjusted to maintain $\Omega_{\text{arp}} = \Omega_{\text{eff}}$ so that in units of t_π, the frequency profile remained the same. Interferometry was then carried out using Raman $\pi/2$ pulses and Raman ARP pulses with $T_\pi = 10t_\pi$ and $T_\pi = 26t_\pi$. A realistic interrogation time of $T = 10$ ms captured contrast loss associated with cloud expansion.

Figure 8 shows that over a 2σ range of the beam radius, the fractional variation in contrast is three times smaller for ARP sweeps than for resonant Raman pulses. While the contrast of the $T_\pi = 10t_\pi$ ARP interferometer still trends with beam position, the more adiabatic $T_\pi = 26t_\pi$ interferometer exhibits just a 1.5% contrast variation out to half the $1/e^2$ intensity radius. This robustness should improve the stability of clock interferometers operating in dynamic environments without the need for larger beam diameters and higher optical power.

C. Sweep parameters

Parameter fluctuations in practical frequency sweeps will introduce instabilities to a Raman ARP-based clock. Variations in Ω_{eff} typically arise from drifts in optical power, polarization, and rf power, whereas perturbations to the sweep parameters T_π, Ω_{arp}, and δ_{max} may result from reproducibility issues associated with broad frequency sweeps in rf systems. To provide a robust timing reference, a Raman ARP Ramsey sequence must withstand reasonable variations in these parameters. Our model predicted <1 mrad phase deviations and contrast variations consistent with zero in response to ±10% changes in the parameters listed above. We experimentally tested the sensitivity by extracting ARP interferograms with $T = 1$ ms interrogation times, while deliberately adjusting the sweep parameters over ±10% of a nominal value (as described in Sec. II). For each parameter, we acquired Raman ARP interferograms with $T_\pi = 10t_\pi$ and $T_\pi = 26t_\pi$. The phase responses plotted in Fig. 9 represent weighted averages, and error bars signify standard errors. Over the ∼1000-s averaging times relevant to these experiments, second-order Zeeman shifts resulting from the large 870-mG bias field limited the long-term stability. At about 4×10^{-11}, the fractional frequency uncertainty of our open-loop clock was consistent with the <3 mrad phase uncertainty seen in this experiment, given a $T = 1$-ms interrogation time. In the next section, we discuss improvements in stability resulting from a reduction in bias field strength.

Due to spontaneous emission, the contrast responded linearly to changes in T_π and Ω_{eff}. The $T_\pi = 26t_\pi$ and $10t_\pi$ cases exhibited maximum contrast deviations of 3.8% and 1.8%, respectively. The maximum respective deviations in background offset were 0.7% and 0.4%. This sensitivity is unlikely to limit a deployed sensor, in which T_π and Ω_{eff} will be controlled to 1% or better. With this stricter bound on pulse parameters, the resulting 0.07% instability in offset yields a fractional frequency stability at 1 s of 3×10^{-13}. These effects will be further suppressed by averaging of sequential phase measurements at $\Delta\varphi = \pm\pi/2$.

By scanning the single-photon Raman laser detuning, we confirmed that spontaneous emission reached a broad minimum between 2 and 3.5 GHz. The magnitude of the detuning scan was bounded by the hyperfine splitting frequency to enable the cancellation of light shifts through the correct choice of optical intensity ratios.

VI. STABILITY ASSESSMENT

To assess the stability of our atomic reference, we computed the Allan deviations of Ramsey frequency measurements based on Raman ARP pulses with $T_\pi = 26t_\pi$, as well as

Raman $\pi/2$ pulses and microwave $\pi/2$ pulses. For these measurements, the bias field was reduced to 87 mG to suppress contributions from environmental magnetic fields. Since the clock state Zeeman shift has a quadratic dependence on field strength, drifts in the magnetic environment, acting in conjunction with a small bias field, produce smaller systematic phase shifts. Phase deviations were related to frequency shifts through precise knowledge of the interrogation time, which was set to $T = 16.667$ ms to synchronize with (and thereby suppress) environmental electromagnetic noise at 60 Hz. Contrast values for the ARP and microwave interferometers were not noticeably changed by the increase in interrogation time from 10 to 16.667 ms. The three pulse types were applied sequentially with a data rate of 1.6 Hz. However, the effective data rate for a particular pulse type was 0.13 Hz, because frequency measurements were based on interferogram fits. Interferograms were extracted from four consecutive measurements with phase shifts of $\Delta\varphi = \{-3\pi/4, -\pi/4, \pi/4, 3\pi/4\}$. This scheme allowed simultaneous measurements of interferometer contrast and background offset. The rf signal generator, provided with a 10-MHz reference from a separate Cs beam clock (Symmetricom 5071A), produced a stable signal that enabled examination of the long-term stability of our atomic reference. The fractional frequency stability of the Cs beam reference is $5 \times 10^{-12}/\sqrt{\tau}$.

The Allan deviations, plotted in Fig. 10(a), indicate that the fractional frequency uncertainty for all interferometers was limited to $\sim 3.5 \times 10^{-12}$ around 2500 s. The similarities in Allan deviations across all pulse types suggest that light shifts were not a limiting factor in this experiment. Subsequent Ramsey spectroscopy with $m_F = 1$ states, which carry first-order sensitivity to the Zeeman shift, revealed magnetic-field instability to be the dominant noise source. In that measurement, Ramsey phase jitter was attributed to magnetic-field fluctuations, which were then used to predict the instability in the clock resonance [see purple diamonds in Fig. 10(a)]. At short averaging times from $\tau = 10$ to 100 s, the slopes of the Allan deviations indicate a white noise process driven largely by the low effective data rate. As shown in Fig. 10(b), frequency measurements acquired at 5 Hz—a 38-fold increase in data rate—improved the short-term stability to $\sim 1.5 \times 10^{-11}$ at $\tau = 1$ s, though white noise was no longer the limiting process. Beyond $\tau = 5$ s, magnetic-field instability once again became the limiting systematic effect. We note that frequency measurements at the higher data rate were based on single shots acquired near quadrature phase and that the pulse types were not interleaved.

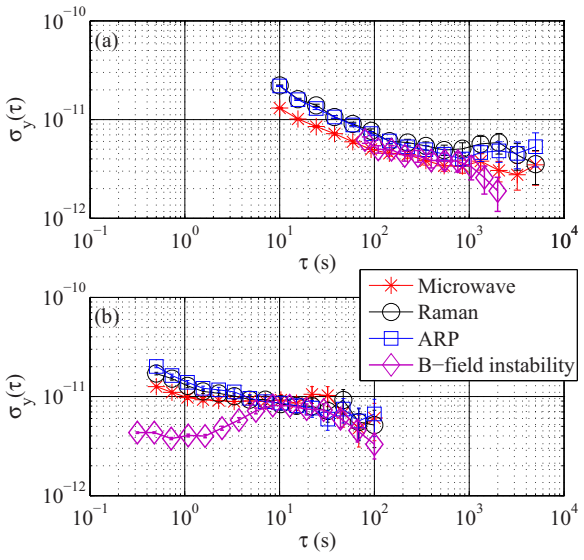

FIG. 10. (Color online) (a) Allan deviations of fractional frequency measurements acquired with three interleaved pulse types. The similarity between the three responses indicates that light shifts were not the limiting systematic effect during this experiment. In our unshielded apparatus, magnetic-field instability was the dominant noise source, as confirmed by Ramsey interrogations of magnetically sensitive m_F states. As a result, the fractional frequency uncertainty was limited to $\sim 3.5 \times 10^{-12}$. (b) Repeating the stability measurement with a higher data rate (5 Hz) improved the short-term stability of all pulse types to $\sim 1.5 \times 10^{-11}$ for an averaging time $\tau = 1$ s. Magnetic fields remained the limiting source of instability for $\tau > 5$ s.

An important source of frequency instability not addressed in this work is atom motion along the Raman beam axis, which Doppler shifts the clock resonance. The Doppler shift could ultimately be measured with a low-cost inertial sensor and compensated by adjusting the Raman detuning. An accelerometer with 10-mg resolution determines the Doppler-induced phase shift to within 1 mrad, limiting the short-term stability to 2×10^{-13} if one assumes an averaging time of 1 s, a sampling rate of 80 Hz, and a Ramsey interrogation time of 10 ms. Alternatively, one could discern Doppler shifts that are stable over consecutive measurements by cycling between forward- and backward-propagating Raman beams. This technique relies on the fact that reversal of beam propagation changes the sign of the Doppler shift but not the clock frequency.

VII. CONCLUSION

We have presented frequency-swept Raman ARP as a tool for robust Ramsey interrogation. With a sufficiently adiabatic sweep, we have produced Raman ARP Ramsey fringes that agree well with those of corresponding sequences based on Raman $\pi/2$ pulses. Raman ARP Ramsey sequences strongly suppress phase sensitivity to light shifts during the pulse. For the small differential ac Stark shifts expected in a practical timing reference ($|\delta_{ac}| \leqslant 0.02\Omega_{eff}$), the phase sensitivity is reduced by about two orders of magnitude, effectively eliminating light shift contributions to short-term noise and improving the prospects for long-term stability with an optical Ramsey interrogation. Our approach also reduces the sensitivity of Ramsey fringe contrast to Gaussian laser beam intensity gradients, which is a critical attribute for cold atom clocks operating in dynamic environments. Potential phase sensitivity to the frequency sweep parameters, if present, is below the resolution limits of our system. Single pulse experiments indicate that the tangent frequency sweep characterized by Eq. (1) is faithfully reproduced by our rf electronics and electro-optics.

Our results suggest Ramsey sequences based on Raman ARP provide a promising path toward realizing a compact primary frequency reference capable of operating in dynamic

environments. Future work will focus on increasing the data rate while maintaining signal-to-noise ratio, adding magnetic shields to suppress ambient field fluctuations, and using our atomic reference to actively stabilize a 10-MHz oscillator.

ACKNOWLEDGMENTS

This work was sponsored by The C. S. Draper Laboratory. K.K. acknowledges support from the Draper Laboratory Fellowship Program.

[1] M. J. Mescher, R. Lutwak, and M. Varghese, in *The 13th International Conference on Solid-State Sensors, Actuators, and Microsystems, 2005. Digest of Technical Papers. TRANSDUCERS '05* (IEEE, Piscataway, NJ, 2005), Vol. 1, pp. 311–316.

[2] R. Lutwak, in *IEEE International Frequency Control Symposium, 2009 Joint with the 22nd European Frequency and Time Forum* (IEEE, Piscataway, NJ, 2009), pp. 573–577.

[3] Microsemi, *Quantum^{TM} SA.45s CSAC data sheet*, 2014.

[4] J. Kitching, L. Hollberg, S. Knappe, and R. Wynands, Electron. Lett. **37**, 1449 (2001).

[5] S. Knappe, V. Shah, P. D. D. Schwindt, L. Hollberg, J. Kitching, L.-A. Liew, and J. Moreland, Appl. Phys. Lett. **85**, 1460 (2004).

[6] T. E. Parker, Metrologia **47**, 1 (2010).

[7] M. A. Kasevich, E. Riis, S. Chu, and R. G. DeVoe, Phys. Rev. Lett. **63**, 612 (1989).

[8] N. Ramsey, Phys. Rev. **78**, 695 (1950).

[9] S. R. Jefferts, J. Shirley, T. E. Parker, T. P. Heavner, D. M. Meekhof, C. Nelson, F. Levi, G. Costanzo, A. De Marchi, R. Drullinger, L. Hollberg, W. D. Lee, and F. L. Walls, Metrologia **39**, 321 (2002).

[10] C. Monroe, H. Robinson, and C. Wieman, Opt. Lett. **16**, 50 (1991).

[11] V. Shah, R. Lutwak, R. Stoner, and M. Mescher, in *IEEE International Frequency Control Symposium (FCS), 2012* (IEEE Piscataway, NJ, 2012), pp. 1–6.

[12] F.-X. Esnault, J. Kitching, and E. A. Donley, in *IEEE International Frequency Control Symposium (FCS), 2012* (IEEE, Piscataway, NJ, 2012), pp. 1–3.

[13] J. Sebby-Strabley, K. Salit, K. Nelson, J. Ridley, and J. Kriz, in *Proceedings of the 43th Annual Precise Time and Time Interval Meeting* (ION, Manassas, VA, 2011), pp. 231–238.

[14] K. Nelson, K. Salit, J. Kriz, D. Sandquist, and J. Sebby-Strabley, in *Position Location and Navigation Symposium (PLANS), 2012 IEEE/ION* (IEEE, Piscataway, NJ, 2012), pp. 1094–1098.

[15] H. J. McGuinness, A. V. Rakholia, and G. W. Biedermann, Appl. Phys. Lett. **100**, 011106 (2012).

[16] F.-X. Esnault, E. Blanshan, E. N. Ivanov, R. E. Scholten, J. Kitching, and E. A. Donley, Phys. Rev. A **88**, 042120 (2013).

[17] E. A. Burt and W. M. Klipstein, in *Proceedings of the IEEE International Frequency Control Symposium and Exposition, 2004* (IEEE, Piscataway, NJ, 2004), pp. 71–79.

[18] J. E. Thomas, P. R. Hemmer, S. Ezekiel, C. C. Leiby, R. H. Picard, and C. R. Willis, Phys. Rev. Lett. **48**, 867 (1982).

[19] B. Young, M. Kasevich, and S. Chu, in *Atom Interferometry*, edited by Paul R. Berman (Academic, San Diego, 1997), pp. 363–406.

[20] R. Stoner, J. Kinast, and B. Timmons, US Patent No. US20130168541 (2013).

[21] J. Bateman and T. Freegarde, Phys. Rev. A **76**, 013416 (2007).

[22] C. J. Hardy, W. A. Edelstein, and D. Vatis, J. Magn. Reson. **66**, 470 (1986).

[23] M. Garwood and L. DelaBarre, J. Magn. Reson. **153**, 155 (2001).

[24] F. Bloch, W. W. Hansen, and M. Packard, Phys. Rev. **69**, 127 (1946).

[25] M. Weitz, B. C. Young, and S. Chu, Phys. Rev. Lett. **73**, 2563 (1994).

[26] L. S. Goldner, C. Gerz, J. C. Spreeuw, S. L. Rolston, C. I. Westbrook, and W. D. Phillips, Phys. Rev. Lett. **72**, 997 (1994).

[27] M. Weitz, B. C. Young, and S. Chu, Phys. Rev. A **50**, 2438 (1994).

[28] D. L. Butts, J. M. Kinast, B. P. Timmons, and R. E. Stoner, J. Opt. Soc. Am. B **28**, 416 (2011).

[29] D. L. Butts, Ph.D. thesis, Massachusetts Institute of Technology, 2012.

[30] R. Stoner, D. Butts, J. Kinast, and B. Timmons, J. Opt. Soc. Am. B **28**, 2418 (2011).

[31] A. Abgragam, *Principles of Nuclear Magnetic Resonance* (Clarendon Press, Oxford, 1996).

[32] J. Baum, R. Tycko, and A. Pines, Phys. Rev. A **32**, 3435 (1985).

[33] T.-L. Hwang, P. C. M. van Zijl, and M. Garwood, J. Magn. Reson. **133**, 200 (1998).

[34] M. Bason, M. Viteau, N. Malossi, P. Huillery, E. Arimondo, D. Ciampini, R. Fazio, V. Giovannetti, R. Mannella, and O. Morsch, Nat. Phys. **8**, 147 (2012).